

Snowflake: A Distributed Streaming Decoder

Tim Chan

Department of Materials, University of Oxford, Parks Road, Oxford OX1 3PH, United Kingdom

We design *Snowflake*, a quantum error correction decoder that runs in a streaming fashion and is capable of a simple, local implementation. In doing so we propose a new method for general stream decoding that eliminates the processing overhead due to window overlap in existing windowing methods. As a first study, we test our local implementation of Snowflake on the surface code under circuit-level noise. It recovers roughly $2/3$ the accuracy threshold of the Union–Find decoder adapted with a windowing method, with a better mean runtime scaling: subquadratic as opposed to cubic in code distance d . We discuss how Snowflake may be implemented on a 2D chip and decode not just quantum memory but lattice surgery-based computation.

1 Introduction

Decoders are crucial to the quantum error correction that enables fault-tolerant quantum computing. These classical algorithms must decode, i.e. infer errors from measurements and fix them, accurately and extremely quickly to clean the quantum computer faster than it corrupts. It is difficult to design a decoder sufficiently accurate, fast, and practical to implement in hardware [1, 2]. This last requirement has led to interest in decoders that are local i.e. running on a grid of identical processors, each communicating only with their nearest neighbours [3–11]. Such decoders benefit from parallelism, hardware practicality [12, §III.D] and robustness [13, §3] when used with local (requiring no long-range qubit–qubit interactions) codes.

A relatively new candidate gaining in popularity [1, 14–18] is the Union–Find decoder (UF) [19, 20]. Recent literature has explored UF implementations of varying levels of locality [13, 21, 22], including *Macar* from [13], which we will repeatedly refer to for comparison. However, these decoders tackled only the batch decoding problem: a simplification of the stream decoding problem that actually happens in practice. Relatively little work has gone into the latter: since 2002, two methods have been proposed allowing most batch decoders to be used as stream decoders. These are the commonly used *forward method*

Tim Chan: timothy.chan@materials.ox.ac.uk

[23, §VI.B] and the newer *sandwich method* [24, 25], using the terminology of [25].

We design Snowflake, a generalisation of the local decoders in [13] from the batch to the streaming case. Snowflake comprises a simple set of local rules with very little central management, and works for any error-correcting code with a decoding graph embeddable in \mathbb{R}^3 without ‘long-range’ edges. Examples include the repetition code and the surface code under circuit-level noise. Snowflake relies on the new *frugal method* we develop for general stream decoding. This is similar to the forward method, but differs in that it discards none of the computation – it is more frugal with resources. This halves both the power draw and the size of the decoder architecture. We hope the proposal of this method enables the development of more streaming decoders.

For the surface code under circuit-level noise, Snowflake has a threshold roughly $2/3$ that of UF adapted with the forward method. Despite its reduced accuracy, Snowflake’s mean runtime scaling with d improves upon original UF. For practical noise levels and code distances, it is roughly as fast as Macar adapted with the forward method. Snowflake also boasts a low-power, distributed implementation that is modular and scalable. This is a 3D lattice of processors; after analysing its runtime, we note an alternative architecture that ‘flattens’ this lattice onto a 2D grid would be even more practical given current chip design capabilities, at potentially a marginal cost in speed.

[Section 2](#) covers the prerequisite theory. In [Section 3](#) we describe the frugal method before explaining Snowflake and its local implementation in [Section 4](#). We numerically test the accuracy and runtime of Snowflake in [Section 5](#), then conclude and discuss how it could decode universal computation in [Section 6](#).

2 Background

[Section 2.1](#) recaps the batch decoding problem that has been previously explained in e.g. [13, §2.1]. In [Section 2.2](#) we generalise to the streaming case and in [Section 2.3](#) we provide one solution approach that already exists in literature.

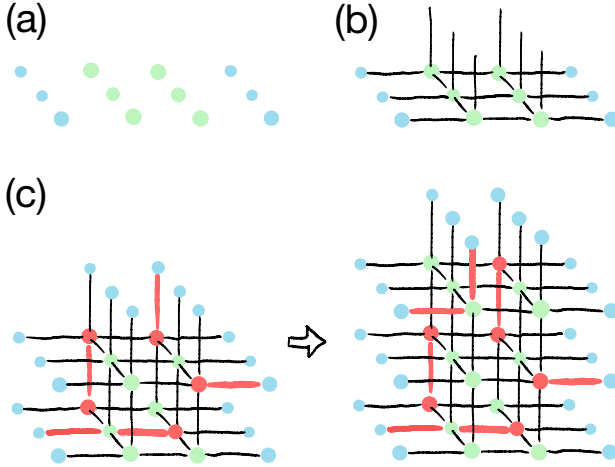


Figure 1: Defects are red nodes; other detectors, green; boundary nodes, blue. Bitflipped edges are thick and red; else, thin and black. (a) A sheet and (b) a layer of the decoding graph for the surface code under phenomenological noise. (c) How said graph changes after one measurement round: one layer is added on top. This is the streaming analogue of the batch version in [13, Figure 3(b)]; note the addition of a temporal boundary.

2.1 The Batch Decoding Problem

The *decoding graph* G is defined by the code and the noise model (we explain how in [Appendix A](#)). Its nodes fall into two types: *detectors*, which can be defects, and *boundary nodes*, which cannot. Each edge is, at any given time, either bitflipped or not bitflipped; this property is not known to the decoder, though it *can* apply bitflips (and of course keep track of which edges it has applied bitflips to).

In a *decoding cycle*, each edge becomes bitflipped with some potentially unique probability that is a function of a universal noise level p .

Definition 1. A *defect* is a detector touching an odd number of bitflipped edges.

The *syndrome* \mathbb{S} is the set of defects. Knowing only \mathbb{S} , the decoder must bitflip more edges, thus modifying \mathbb{S} , until $\mathbb{S} = \emptyset$. The decoding cycle ends here. Formally, be the *correction* \mathbb{C} the final set of edges the decoder chooses to bitflip; then \mathbb{C} must *annihilate all defects* i.e. constitute paths that pair each defect with either another defect or a boundary node.

A *logical bitflip* is a path of bitflipped edges between opposite boundaries. We evaluate decoder accuracy by the probability a single batch fails i.e. a single decoding cycle ends with an odd number of logical bitflips leftover.

2.2 The Stream Decoding Problem

Whereas the batch decoding problem was defined for three noise models, this problem is defined for only two of them: phenomenological and circuit-level.

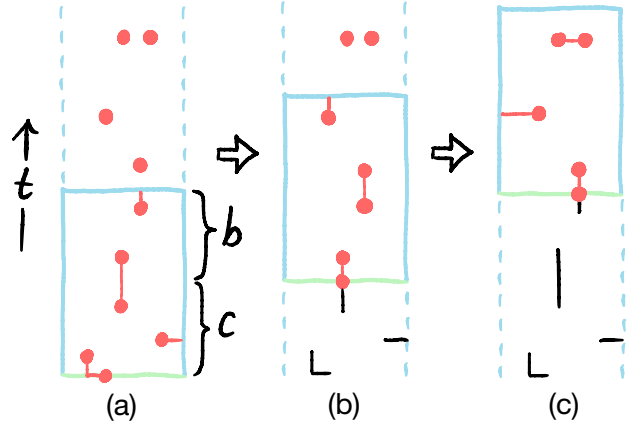


Figure 2: Two decoding cycles of the forward method. The viewing window is the solidly outlined rectangle with boundaries in blue. Defects are red dots. Tentative corrections are red lines; edges bitflipped by the decoder, black lines. The commit and buffer region heights are c and b , respectively. (a) The tentative correction contains a path that spans both regions. (b) This path is partially committed which makes an ‘artificial defect’ at the bottom of the new window that must also be annihilated. (c) The rest of the path is committed.

[Figure 1\(a, b\)](#) illustrates the following definitions: a *sheet* is a subset of nodes of G with the same t coordinate; a *layer*, the periodic unit subgraph of G . For the stream decoding problem, there are an *indefinite* number of measurement rounds; this means new layers are constantly being added to the top of G as in [Fig. 1\(c\)](#). In general, some edges in the new layer are bitflipped (specifically, the bitflip probability for each edge equals that of the analogous edge in the layer below), creating defects in the new layer. The decoder must constantly add to \mathbb{C} to annihilate these new defects.

We evaluate decoder accuracy by the below metric which is a reasonable streaming analogue to the batch failure probability.

Definition 2. The *logical error rate* is the logical bitflip count per d measurement rounds.

For visual clarity, the figures in the rest of this paper, save [Section 5](#), show a planar G corresponding to the repetition code under phenomenological noise. However, the same concepts apply to other graphs such as for the surface code under circuit-level noise. The time axis always points upward.

2.3 Forward Method

This method was first proposed in [23, §VI.B] as the ‘overlapping recovery method’ but a more detailed explanation can be found in [24, pp 2–3] where it is called ‘sliding window decoding’. It reduces the stream decoding problem to batch decoding by chunking the syndrome, decoding each chunk, then stitching together all the corrections. The chunks must overlap,

else a small defect pair could straddle two consecutive chunks hence be decoded inaccurately.

More concretely, assume G already comprises many layers. This method, illustrated in [Fig. 2](#), relies on a ‘viewing window’ W that is at any given time a subgraph comprising $c+b$ consecutive layers of G . The lowest c layers of W is always defined as the *commit region*; the rest, the *buffer region*. W starts at the bottom, i.e. as the lowest $c+b$ layers, of G . The method then indefinitely repeats the decoding cycle, defined as the following:

1. Use any batch decoder to find a *tentative correction* \mathbb{T} that annihilates all defects seen in W .
2. Add to \mathbb{C} the part of \mathbb{T} in the commit region, and forget the rest.
3. Raise W by c layers i.e. redefine it as the subgraph that is c layers higher.

Since b ‘layers of computation’ are forgotten per decoding cycle, decoding τ sheets of syndrome data discards a total of $\approx b\tau/c$ layers of computation. If the bitflip probabilities of all edges of G are of the same order, we need the chunk overlap $b \gtrsim d$ (a common choice is $c = b = d$). Thus a considerable amount of computation is discarded. This is true for the sandwich method too which also requires overlapping windows.

Remark 1. Having a temporal boundary at the top of W improves decoding accuracy [\[25, §B.3\]](#) as it allows the decoder to account for small defect pairs that straddle this boundary like the one in [Fig. 2\(a\)](#). By tentatively pairing the known defect to the temporal boundary, the decoder delays the decision on how to properly annihilate it until it discovers the other defect just above in (b). The same occurs with another defect near the top of W in (b), but this time it turns out there are no nearby defects above, so it is instead paired to a spatial boundary in (c).

3 Frugal Method

Our alternative to the forward method differs from it in three ways:

1. \mathbb{T} need only satisfy the following.

Condition 1. \mathbb{T} is *complete*, i.e. annihilates all defects, within the commit region.

This is as opposed to being complete in *all* of W .

2. The decoder bitflips *all* edges in \mathbb{T} , modifying \mathbb{S} even in the buffer region during [step 1](#). This has no physical consequence for qubits as \mathbb{C} is ultimately only tracked by classical electronics in the so-called Pauli frame [\[26, 27\]](#).

3. The computation associated with the buffer region is not forgotten but used as a starting point for, and further developed in, the next decoding cycle.

As computation is never discarded, the power draw and thus heat generated by the device is minimised. This is vital for an on-chip, local decoder integrated with the qubits, as most qubit platforms demand low temperatures. Compared to the forward method for $c = b$, where 1 layer of computation is discarded per sheet of syndrome data, the power draw is halved.

Ideally, each decoding cycle would complete faster than c ancilla qubit measurement intervals. In practice, we can demand less from the decoder by introducing a buffer (in the conventional sense) between the newest measurement data and the top of W , in which case only *an average* decoding cycle would need to complete faster than c intervals. Any slower then the backlog of syndrome data grows indefinitely [\[12, p 326\]](#). We analyse this average for Snowflake in [Section 5.2](#).

For the rest of the paper we set $c = 1$, which we can do for free as computation is never discarded. In this case the method becomes local (provided the decoder itself is local) as, from the perspective of W , data shifts down by *one layer* when W is raised. The commit region is also one layer thick, so the part of \mathbb{C} here can be offloaded from the bottom of W locally. Conceptually, this makes the method much more granular in nature.

4 Snowflake

[Figure 3](#) illustrates how our local decoder finds \mathbb{T} . The algorithm is inspired by UF and explained by analogy to snowfall. As snowflakes fall they gradually grow. If two snowflakes touch they merge i.e. become one. In the same way, an active cluster nucleates at each new defect at the top of W and grows as it fall through W . If two clusters touch they merge.

A cluster stops growing if it inactivates. We use the following lemma from [\[13, §A.2\]](#).

Lemma 1. *A cluster is inactive iff it has an even defect count or touches a boundary.*

To determine the first condition, we push all defects to a unique point in the cluster called the *root*: a boundary if available; else, a highest point. When two defects meet they annihilate, so eventually zero or one defect will remain, indicating the defect count parity.

To ‘push a defect’ we simply bitflip the edge we want to push it along (this is consistent with [Definition 1](#) and with the previous paragraph: if there is a defect at the other end of the edge, they annihilate). This way, \mathbb{T} is the symmetric difference of all

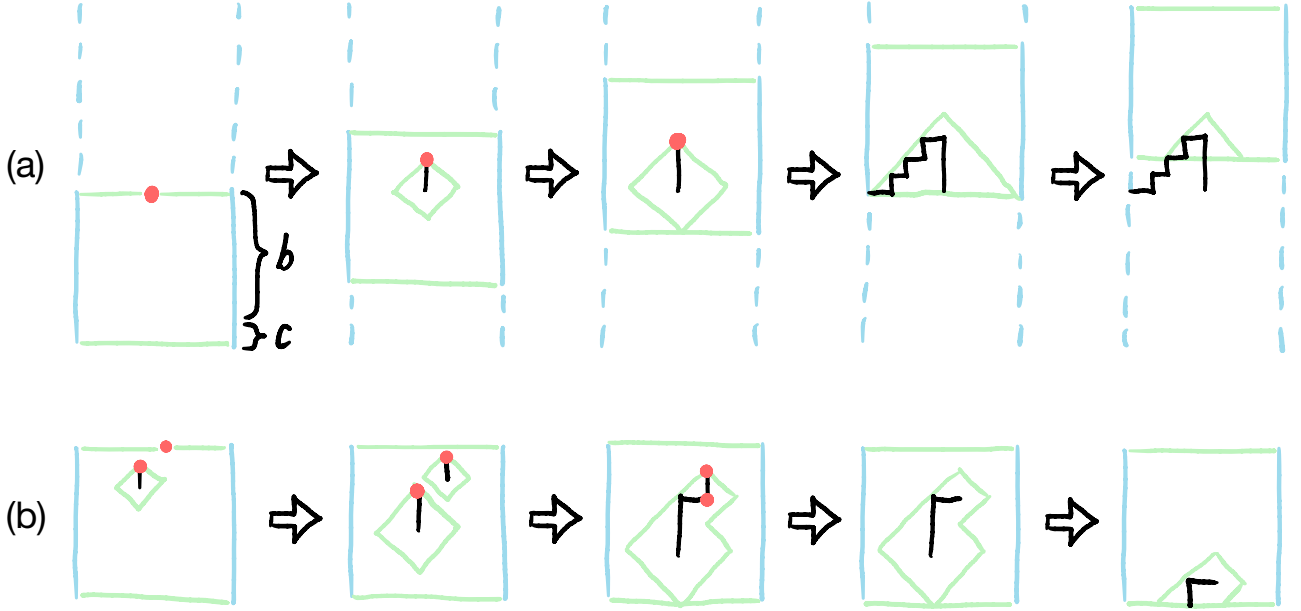


Figure 3: Two examples of Snowflake in action. Features are shown as in Fig. 2 and additionally, clusters are outlined in green. (a) A cluster grows around one defect as the window is raised, while the defect is always pushed to the highest point. As soon as the cluster touches a boundary, the defect is instead pushed to that boundary. This inactivates the cluster so it stops growing. It gradually disappears from view. (b) Two defects separated in time and space (this time viewed from the perspective of the window so clusters appear to fall). The lower cluster is older, hence larger, when both clusters merge. Frame 3 shows the lower defect on its way to the highest point to annihilate with the other defect, inactivating the resultant cluster.

the paths traced by defects and moreover is guaranteed to be complete within any inactive cluster. The idea then is to inactivate all clusters once they have fallen far enough.

Snowflake performs one growth round per decoding cycle. This comprises growing each active cluster in all possible (defined by the edges of G) directions by half an edge, merging touching clusters and pushing defects to roots. Even despite Remark 1 we define $W = (V_W, E_W)$ sans temporal boundary because clusters fall twice as fast as they grow so this boundary would never be touched.

The height of the buffer region is lower-bounded by the following.

Proposition 1. *The minimum layer count of the buffer region that guarantees Condition 1, is $b_{\min} := 2\lfloor d/2 \rfloor$.*

Proof. Defects are annihilated by either meeting another defect or being pushed to a boundary. So a longest-living defect is one like that in Fig. 3(a): never meeting another defect, and created as far as possible, i.e. $\lfloor d/2 \rfloor$ edges, from any boundary. The cluster containing this defect grows outward by half an edge per growth round so will touch a boundary after b_{\min} growth rounds, at the $(b_{\min} + 1)^{\text{th}}$ layer from the top. So T is always complete in this layer and below, but not above. \square

We set $b = b_{\min}$ for our local implementation. Minimising c and b in the frugal method roughly halves

the height of W compared to the forward method for $c = b = d$. We will see in the next subsection this halves the processor count of our implementation.

4.1 Local Implementation

We use the same local architecture of Macar and Actis in [13] i.e. a processor for each node in V_W , a communication link for each edge and one controller which manages the global variables of the algorithm. For the surface code, the processors and links form a 3D lattice, oriented so the time axis points upward like in Fig. 3(b).

Snowflake is compatible with any choice of network for controller–processor communication, be it the hierarchical tree used in Macar or the strictly local staging and signalling tree in Actis, with synchronous or asynchronous logic. We thus leave it as an implementation choice.

Our implementation follows discrete timesteps with each component performing one operation, and messages travelling one link, per timestep. Appendix B provides the rest of the details.

5 Numerics

We emulate the memory experiment (preserving a logical qubit) for our local implementation of Snowflake on the surface code under the circuit-level noise model detailed in [13, §B]. Specifically, we decode the syndrome from nd measurement rounds for a large integer

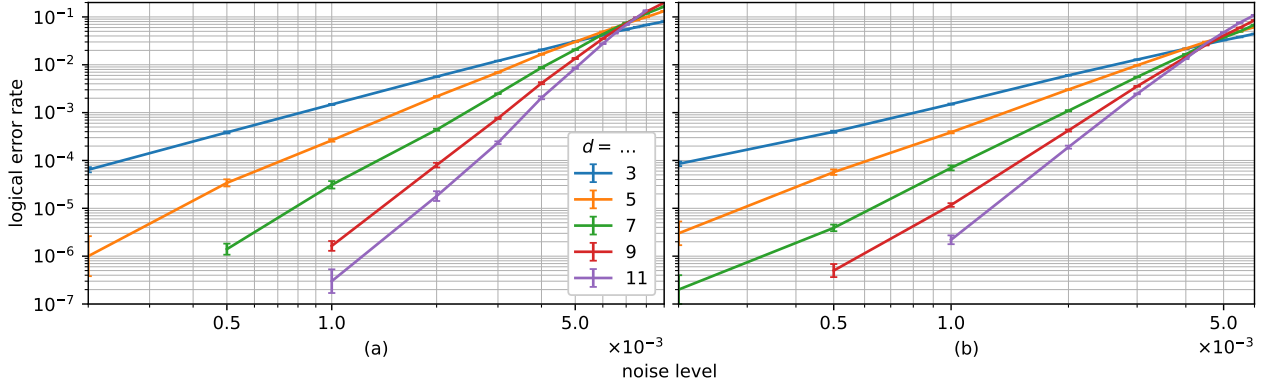


Figure 4: Threshold plots for (a) UF adapted with the forward method and (b) Snowflake, both applied to the surface code of distance d under circuit-level noise. Each datapoint is the mean of $10^5\text{--}2 \cdot 10^7$ lots of d measurement rounds; errorbars show standard error. The *logical error rate* is the logical bitflip count per d measurement rounds.

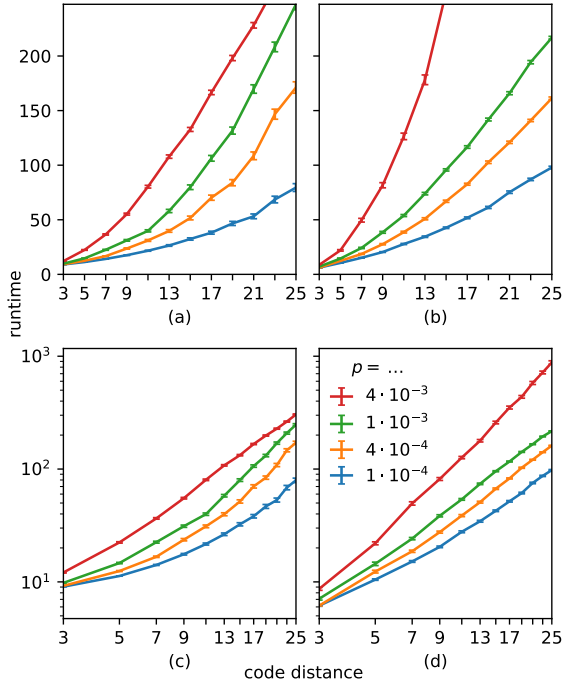


Figure 5: Decoder timestep count per d measurement rounds against surface code distance d , for various circuit-level noise levels p below threshold (red is only marginally below Snowflake’s threshold). Each datapoint is the mean of 10^2 lots of d measurement rounds; errorbars show standard error. (a) Macar [13] adapted with the forward method. (b) Snowflake. (c, d) same as (a, b) but on a log–log scale.

Table 1: Gradient m of the lines in Fig. 5(d) estimated using Weighted Least Squares.

p	m
10^{-4}	1.30(4)
$4 \cdot 10^{-4}$	1.55(3)
10^{-3}	1.68(2)
$4 \cdot 10^{-3}$	2.20(3)

n , then count one of two features depending on if we are benchmarking accuracy or runtime.

5.1 Accuracy

For this we count the number m of logical bitflips in the leftover. We identify these paths between opposite boundaries with a new method we describe in a paper currently in preparation. We then estimate the logical error rate $\hat{f} = m/n$ as per [Definition 2](#).

[Figure 4](#) compares the accuracy of UF (adapted with the forward method) and Snowflake, for practical noise levels and code distances. The former has a threshold of $\approx 7.3 \cdot 10^{-3}$ while Snowflake has a threshold of $\approx 4.6 \cdot 10^{-3}$. This discrepancy comes from the difference in relative cluster sizes e.g. were UF used in [Fig. 3\(b\)](#), both clusters would be the same size when they merge. For future work, Snowflake could try recover this behaviour by growing newer, smaller clusters faster to improve accuracy.

5.2 Runtime

For this we count the number of timesteps to decode, per d measurement rounds. We normalise by d rounds as each logical operation lasts $\mathcal{O}(d)$ rounds using lattice surgery [28], the best known technique for universal computation with the surface code when the quantum device has local connectivity [29, 30].

[Figure 5](#) compares the runtime of Macar and Snowflake. We exclude their controller–processor communication cost by assuming implementations where the controller connects directly to each processor. To adapt Macar to the streaming case, we measure its runtime to decode a viewing window with $c = b = d$, then add c timesteps due to [step 3](#) of the forward method.

We make two observations. First, Macar is considerably slower decoding a batch of $2d$ compared to d sheets of syndrome data. Moreover, its runtime no

longer scales sublinearly in d , as Fig. 5(a) shows (cf. [13, Figure 12(a)]). Second, Macar and Snowflake are roughly the same speed in the practical, i.e. $p \lesssim 10^{-3}$, noise level regime.

Using the data on Snowflake, Table 1 estimates the scaling m , assuming its mean runtime $\propto d^m$ i.e. that the lines in Fig. 5(d) are straight [not the case for Macar in (c)]. We see for practical noise levels that the scaling is subquadratic: better than the slightly-higher-than-cubic scaling [21, §2.3] of original UF but worse than the sublinear scaling [13] of Macar when decoding a batch as tall as Snowflake’s viewing window. We suspect that this is because for Macar, active clusters in the same batch all grow at the same time regardless of their vertical coordinate. In Snowflake, this process is somewhat serialised: older active clusters start growing before newer ones do, as they enter W earlier; see e.g. Fig. 3(b).

This serialisation in the vertical direction suggests the viability of an alternative architecture: ‘flattening’ the 3D lattice down onto a 2D grid so there is one processor for each *set of nodes* of the same (x, y) coordinate i.e. each ancilla qubit. This comes at the cost of serialising the operations within each set, but if these operations are inherently serial, the cost could be marginal. There are two benefits: first, it is more practical as a 2D chip is far easier to build than a 3D lattice of processors; second, messages passed vertically would be instantaneous within a timestep. We leave emulation and numerical analysis of this flattened implementation as future work.

6 Conclusion

We propose the frugal method for stream decoding of quantum error-correcting codes for which there exists a decoding graph embeddable in \mathbb{R}^3 without ‘long-range’ edges. We design Snowflake, a simple decoder compatible with this method and numerically benchmark its local implementation.

As this paper is a first study, there are various avenues of further investigation (in addition to the ones mentioned so far) for the frugal method and Snowflake.

Asynchronous Logic As discussed in [13, §6], controller–processor communication could run by asynchronous (instead of synchronous) logic, which would speed up Snowflake. One could explore which other processes in Snowflake could be sped up by asynchronous logic.

Weighted Edges Clusters could grow along edges at different speeds to account for their different bit-flip probabilities, which would improve accuracy [15]. These speeds could even be configurable in the hardware to fine-tune the noise model during a calibration

stage; this however would alter Proposition 1, requiring b_{\min} to also be configurable, which is nontrivial.

Computation Recently, the sandwich method has been generalised from quantum memory to lattice surgery computation [31–33]. We propose an alternative approach to decoding lattice surgery that exploits the granular and local nature of Snowflake. Imagine the decoder as a homogeneous substrate positioned just above the whole 2D lattice of qubits. Regions of this substrate are turned on (to decode) wherever the below qubits are involved in surgery. Snowflake would work best with the so-called *twist-free* lattice surgery [34, §IV] which avoids using any elongated (hence nonlocal) stabilisers. Some details of the local implementation in Appendix B.1 would need to be generalised. E.g. since boundaries vary during lattice surgery, the ID of each processor would no longer be a constant integer; rather, a combination of a constant 3D coordinate and a (relative) variable boolean indicating whether the processor represents a boundary node. This preserves Remark 2. For controller–processor communication, a hierarchical tree like that used in Macar would be best, as communication cost would then scale logarithmically with the length of the qubit lattice, which may be much larger than d .

Acknowledgments

I thank Simon Benjamin and Matt Cassie for useful discussions. I acknowledge the use of the University of Oxford Advanced Research Computing (ARC) facility [35] in carrying out this work and specifically the facilities made available from the EPSRC QCS Hub grant (agreement No. EP/T001062/1). I also acknowledge support from an EPSRC DTP studentship and two EPSRC projects: RoaRQ (EP/W032635/1) and SEEQA (EP/Y004655/1). Open-source Python libraries used in this work include `matplotlib`, `networkx`, `numpy`, `pandas`, `pytest`, `scipy`, `statsmodels`.

References

- [1] Poulami Das, Christopher A. Pattison, Srilatha Manne, Douglas M. Carmean, Krysta M. Svore, Moinuddin Qureshi, and Nicolas Delfosse. “AFS: Accurate, fast, and scalable error-decoding for fault-tolerant quantum computers”. In 2022 IEEE International Symposium on High-Performance Computer Architecture (HPCA). Pages 259–273. (2022).
- [2] Nicolas Delfosse, Andres Paz, Alexander Vaschillo, and Krysta M. Svore. “How to choose a decoder for a fault-tolerant quantum computer? the speed vs accuracy trade-off” (2023). [arXiv:2310.15313](https://arxiv.org/abs/2310.15313).

[3] James William Harrington. “Analysis of quantum error-correcting codes: symplectic lattice codes and toric codes”. *PhD thesis*. California Institute of Technology. (2004).

[4] Austin G. Fowler. “Minimum weight perfect matching of fault-tolerant topological quantum error correction in average $O(1)$ parallel time” (2014). [arXiv:1307.1740](https://arxiv.org/abs/1307.1740).

[5] Michael Herold, Earl T. Campbell, Jens Eisert, and Michael J. Kastoryano. “Cellular-automaton decoders for topological quantum memories”. *npj Quantum Information* **1**, 15010 (2015).

[6] Nikolas P. Breuckmann, Kasper Duivenvoorden, Dominik Michels, and Barbara M. Terhal. “Local decoders for the 2D and 4D toric code” (2016). [arXiv:1609.00510](https://arxiv.org/abs/1609.00510).

[7] Michael Herold, Michael J. Kastoryano, Earl T. Campbell, and Jens Eisert. “Cellular automaton decoders of topological quantum memories in the fault tolerant setting”. *New Journal of Physics* **19**, 063012 (2017).

[8] Nicolai Lang and Hans Peter Büchler. “Strictly local one-dimensional topological quantum error correction with symmetry-constrained cellular automata”. *SciPost Physics* **4**, 007 (2018).

[9] Aleksander Kubica and John Preskill. “Cellular-automaton decoders with provable thresholds for topological codes”. *Physical Review Letters* **123**, 020501 (2019).

[10] Nicolas Delfosse. “Hierarchical decoding to reduce hardware requirements for quantum computing” (2020). [arXiv:2001.11427](https://arxiv.org/abs/2001.11427).

[11] Samuel C. Smith, Benjamin J. Brown, and Stephen D. Bartlett. “Local predecoder to reduce the bandwidth and latency of quantum error correction”. *Physical Review Applied* **19**, 034050 (2023).

[12] Barbara M. Terhal. “Quantum error correction for quantum memories”. *Review of Modern Physics* **87**, 307–346 (2015).

[13] Tim Chan and Simon C. Benjamin. “Actis: A strictly local Union–Find decoder”. *Quantum* **7**, 1183 (2023).

[14] Muyuan Li, Daniel Miller, Michael Newman, Yukai Wu, and Kenneth R. Brown. “2D compass codes”. *Physical Review X* **9**, 021041 (2019).

[15] Shilin Huang, Michael Newman, and Kenneth R. Brown. “Fault-tolerant weighted union-find decoding on the toric code”. *Physical Review A* **102**, 012419 (2020).

[16] Shui Hu. “Quasilinear time decoding algorithm for topological codes with high error threshold”. *Master’s thesis*. Delft University of Technology. (2020).

[17] Ben Barber, Kenton M. Barnes, Tomasz Bialas, Okan Buğdayci, Earl T. Campbell, Neil I. Gillespie, Kauser Johar, Ram Rajan, Adam W. Richardson, Luka Skoric, Canberk Topal, Mark L. Turner, and Abbas B. Ziad. “A real-time, scalable, fast and highly resource efficient decoder for a quantum computer” (2023). [arXiv:2309.05558](https://arxiv.org/abs/2309.05558).

[18] Sam J. Griffiths and Dan E. Browne. “Union-find quantum decoding without union-find”. *Physical Review Research* **6**, 013154 (2024).

[19] Nicolas Delfosse and Gilles Zémor. “Linear-time maximum likelihood decoding of surface codes over the quantum erasure channel”. *Physical Review Research* **2**, 033042 (2020).

[20] Nicolas Delfosse and Naomi H. Nickerson. “Almost-linear time decoding algorithm for topological codes”. *Quantum* **5**, 595 (2021).

[21] Namitha Liyanage, Yue Wu, Alexander Deters, and Lin Zhong. “Scalable quantum error correction for surface codes using FPGA” (2023). [arXiv:2301.08419](https://arxiv.org/abs/2301.08419).

[22] Maximilian Jakob Heer, Emanuele Del Sizzo, Keisuke Fujii, and Kentaro Sano. “Novel union-find-based decoders for scalable quantum error correction on systolic arrays”. In 2023 IEEE International Parallel and Distributed Processing Symposium Workshops (IPDPSW). *Pages* 524–533. (2023).

[23] Eric Dennis, Alexei Kitaev, Andrew Landahl, and John Preskill. “Topological quantum memory”. *Journal of Mathematical Physics* **43**, 4452–4505 (2002).

[24] Luka Skoric, Dan E. Browne, Kenton M. Barnes, Neil I. Gillespie, and Earl T. Campbell. “Parallel window decoding enables scalable fault tolerant quantum computation”. *Nature Communications* **14**, 7040 (2023).

[25] Xinyu Tan, Fang Zhang, Rui Chao, Yaoyun Shi, and Jianxin Chen. “Scalable surface-code decoders with parallelization in time”. *PRX Quantum* **4**, 040344 (2023).

[26] Emanuel Knill. “Quantum computing with realistically noisy devices”. *Nature* **434**, 39–44 (2005).

[27] L. Riesenbos, X. Fu, S. Varsamopoulos, C. G. Almudever, and K. Bertels. “Pauli frames for quantum computer architectures”. In Proceedings of the 54th Annual Design Automation Conference 2017. *Pages* 1–6. New York, NY, USA (2017). Association for Computing Machinery.

[28] Dominic Horsman, Austin G. Fowler, Simon Devitt, and Rodney Van Meter. “Surface code quantum computing by lattice surgery”. *New Journal of Physics* **14**, 123011 (2012).

[29] Austin G. Fowler and Craig Gidney. “Low overhead quantum computation using lattice surgery” (2019). [arXiv:1808.06709](https://arxiv.org/abs/1808.06709).

[30] Daniel Litinski. “A game of surface codes: Large-scale quantum computing with lattice surgery”. *Quantum* **3**, 128 (2019).

[31] Craig Gidney. “Stability experiments: The overlooked dual of memory experiments”. *Quantum* **6**, 786 (2022).

[32] Héctor Bombín, Chris Dawson, Ye-Hua Liu, Naomi Nickerson, Fernando Pastawski, and Sam Roberts. “Modular decoding: parallelizable real-time decoding for quantum computers” (2023). [arXiv:2303.04846](https://arxiv.org/abs/2303.04846).

[33] Sophia Fuhui Lin, Eric C. Peterson, Krishanu Sankar, and Prasahnt Sivarajah. “Spatially parallel decoding for multi-qubit lattice surgery” (2024). [arXiv:2403.01353](https://arxiv.org/abs/2403.01353).

[34] Christopher Chamberland and Earl T. Campbell. “Universal quantum computing with twist-free and temporally encoded lattice surgery”. *PRX Quantum* **3**, 010331 (2022).

[35] Andrew Richards. “University of Oxford Advanced Research Computing”. (2015).

A What the Decoding Graph Represents

Since the stream decoding problem is defined for only phenomenological and circuit-level noise, we explain what G physically represents under these two models.

Each detector represents the difference between two consecutive measurements of an ancilla qubit at a given point in time. Boundary nodes represent nothing physical.

There are two types of edges: bulk edges, which are not incident to a boundary node, and boundary edges, which are. Each bulk (boundary) edge represents a possible pair of defects (a possible defect) that could have resulted from one fault. A *fault* is defined for phenomenological noise as either a data qubit bitflip or a measurement outcome flip; for circuit-level noise, an error process in the syndrome extraction circuit.

Note G allows for correcting only bitflips i.e. \hat{X} errors. The full decoding problem in practice requires another similar-looking but independent decoding graph (with its own separate decoder) to allow for correcting phaseflips i.e. \hat{Z} errors.

B Local Implementation of Snowflake

In this section we refer to processors as nodes and communication links as edges. The controller can broadcast the same boolean to, and receive (without knowing the sender) booleans from, every node.

Algorithm 1 Run by controller every timestep.

```
if not (waiting or any  $v.\text{busy}$ ) then
  for all  $v \in V_W$  do
     $v.\text{stage} \leftarrow \text{drop}$ 
    wait 2 timesteps
```

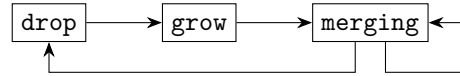


Figure 6: Flowchart for the stages of Snowflake: `drop` and `grow` each last one timestep whereas `merging` lasts a variable number, hence the loop on `merging`. Snowflake cycles through all three stages once per decoding cycle.

Algorithm 2 Run by node v every timestep.

```
if  $v.\text{stage} = \text{drop}$  then
   $\text{DROP}(v)$ 
   $v.\text{stage} \leftarrow \text{grow}$ 
else if  $v.\text{stage} = \text{grow}$  then
   $\text{GROW}(v)$ 
   $v.\text{stage} \leftarrow \text{merging}$ 
else
   $\text{MERGING}(v)$ 
```

In [Appendix B.1](#) we list the variables each component stores and in [Appendix B.2](#) we explain how they are manipulated in order to effect Snowflake.

B.1 Setup

Each node $v \in V_W$ is assigned a unique integer ID and stores the following variables:

- `active` is a boolean indicating whether the cluster that v is in is active. If $v.\text{active} = \text{true}$ we say v is active.
- `CID` is an integer indicating the cluster that v belongs to. Clusters are identified by the lowest ID of all its nodes. The node of this ID is the root. `CID` can also adopt the value `reset` to indicate v should `unroot` (defined in [Appendix B.2.2](#)) in the next timestep.
- `defect` is a boolean indicating whether v has a defect. This can be thought of as a particle which is passed between nodes. When a node receives two defects in a timestep, they annihilate.
- `pointer` is the direction v should push the defect (by bitflipping the corresponding edge). Possible values (under circuit-level noise) are `C`, `N`, `W`, `E`, `S`, `D`, `U`, `NU`, `WD`, `EU`, `SD`, `NWD`, `SEU`, representing respectively centre, north, west, east, south, down, up, and combinations thereof. Following the pointers starting from v should eventually lead to the root of the cluster that v is in. Only roots have `pointer = C` as they do not push defects but accumulate them.
- `unrooted` is a boolean indicating whether v has unrooted in the current decoding cycle.
- `busy` is a boolean indicating whether v is busy.
- `stage` is the current stage of Snowflake. This follows the flowchart in [Fig. 6](#).

Algorithm 3 Procedures for [Algorithm 2](#).

```

procedure DROP( $v$ )
2:    $v.\text{unrooted} \leftarrow \text{false}$ 
3:   for  $e \in v.\text{owned} \cap \text{commit region}$  do
4:     if  $e.\text{correction}$  then ▷ Commit  $e$ .
5:        $\mathbb{C} \leftarrow \mathbb{C} \Delta \{e\}$ 
6:     if  $\exists$  node  $u$  below  $v$  then ▷ Shift relative data down one layer.
7:        $v.\text{CID} \leftarrow \text{ID of node below current root}$ 
8:       send all relative variables to  $u$ 
9:     if  $v \in \text{top sheet of } W$  then ▷ Inherit the new measurement round results.
10:       $v.\text{defect} \leftarrow \text{whether the measurement of the corresponding ancilla qubit differs from the last round}$ 
11:       $v.\text{active} \leftarrow \text{false}$ 
12: procedure GROW( $v$ )
13:   if  $v.\text{active}$  then
14:     for all unfully grown edges  $e$  incident to  $v$  do ▷ Start unrooting  $v$ .
15:        $e.\text{growth} \leftarrow e.\text{growth} + \frac{1}{2}$ 
16:     if  $v \in \text{bottom sheet of } W$  and  $v.\text{pointer} \ni \mathbb{D}$  then
17:        $v.\text{CID} \leftarrow \text{reset}$ 
18:        $v.\text{pointer} \leftarrow \mathbb{C}$ 
19: procedure MERGING( $v$ )
20:    $v.\text{busy} \leftarrow \text{false}$ 
21:   SYNCING( $v$ )
22:   FLOODING( $v$ )

```

We refer to the first four variables as *relative* and the last three as *absolute*. Each edge $e \in E_W$ has the following variables:

- **growth** is its growth value which is in $\{0, \frac{1}{2}, 1\}$. Two clusters touch when they become connected via a fully grown edge.
- **correction** is a boolean indicating if $e \in \mathbb{T}$.

These are stored as additional relative variables at the endpoint with the lower ID. It helps to define the *owned edges* as those whose variables a node stores:

$$v.\text{owned} := \{uv : uv \in E_W \text{ and } v.\text{ID} < u.\text{ID}\}. \quad (1)$$

B.2 Procedures

Though the pseudocode in this subsection explains exactly what each component does, it is difficult to infer from this the *emergent effect*. We describe the latter in the accompanying prose.

In each timestep the controller runs [Algorithm 1](#), which tells all nodes to start a new decoding cycle if none of them are busy during merging. This is the only time the controller needs to communicate with the nodes, as merging is the only variable-duration stage.

At the same time, each node v runs [Algorithm 2](#), calling procedures from [Algorithm 3](#). Stage `drop` adds to \mathbb{C} and raises W by one layer, as in [Fig. 7\(a–b\)](#). Each node v in the top sheet of W starts in its own

cluster, thus sets its relative variables to reflect this ([Lines 10 and 11](#)). $v.\text{CID}$ and $v.\text{pointer}$ need not be explicitly reset as they never change from their correct values of $v.\text{ID}$ and \mathbb{C} , respectively. Stage `grow` grows all edges around each active cluster by $\frac{1}{2}$, as in [Fig. 7\(b–c\)](#).

B.2.1 Merging

[Figure 7\(c–f\)](#) shows a `merging` example which needs three timesteps. This stage comprises two processes, syncing and flooding, which occur independently. We thus split `MERGING` into two subroutines, given in [Algorithm 4](#), effecting each process.

In flooding, newly touching clusters adopt the lowest **CID** among them. This **CID** propagates as a flood starting from where they touched: each node looks at its neighbours along fully grown edges. If it sees a lower **CID** than its own, it adopts that **CID** and points toward that neighbour ([Lines 28 to 31](#)). After this process, all nodes in a given cluster will have the same **CID**, and following the pointers will always lead to the root promised by **CID**.

Remark 2. Crucial to the algorithm is that boundary nodes are of lower ID than detectors. Each root can thus determine if its cluster touches a boundary by checking if itself is a boundary node.

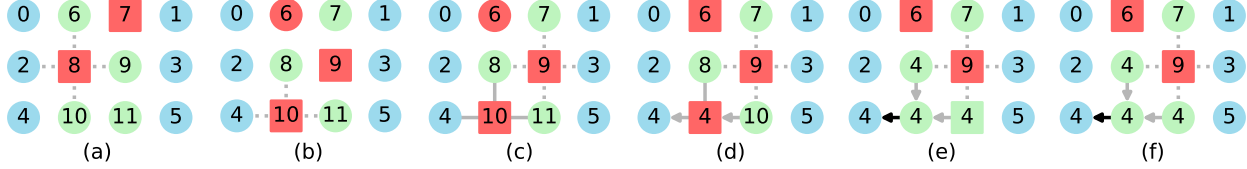


Figure 7: A decoding cycle example for a distance-3 code. Active nodes are squares; inactive nodes, circles. CID is shown as a label. Ungrown edges are invisible; half-grown, dotted; fully grown, solid. Pointers are shown by arrows on edges. Edges bitflipped by the decoder are in black. (a) Each node is in its own cluster so has $\text{CID} = \text{ID}$. Two clusters are active. (b) During drop, *all* relative variables fall by one layer, including CID which is adjusted to refer to the node below. A new defect appears at the top. (c) During grow, each active node grows its incident edges by $\frac{1}{2}$. Nodes 10 and 11 now each see a lower CID than their own when they look at their neighbours along fully grown edges. (d) merging starts. They adopt that CID and point toward that neighbour; node 8 thus sees a lower CID than its own. Node 6 recognises it is a root with a defect, so becomes active. (e) A defect is pushed along a pointer to the root which bitflips an edge. Node 8 updates its CID and pointer, so now the 4-node cluster is fully flooded but not yet fully synced. (f) Throughout merging, each non-root node was adopting the active variable of the node it was pointing to. This activity propagation now completes, so the 4-node cluster is fully synced.

Algorithm 4 Subroutines for MERGING.

```

procedure SYNCING( $v$ )
2:    $x := (v \text{ is a detector}) \text{ and } v.\text{defect}$ 
   if  $v.\text{pointer} = C$  then  $\triangleright v \text{ is a root.}$ 
4:      $v.\text{active} \leftarrow x$ 
   else
6:      $u := \text{node toward } v.\text{pointer}$ 
      $v.\text{active} \leftarrow u.\text{active}$ 
8:     if  $x$  then
        $v.\text{busy} \leftarrow \text{true}$ 
10:    flip  $uv.\text{correction}$  to push defect to  $u$ 
   if  $v.\text{active}$  changed then
12:     $v.\text{busy} \leftarrow \text{true}$ 

14: procedure FLOODING( $v$ )
   if  $v.\text{CID} = \text{reset}$  then  $\triangleright \text{Finish unrooting } v.$ 
16:    $v.\text{busy} \leftarrow \text{true}$ 
    $v.\text{CID} \leftarrow v.\text{ID}$ 
18:    $v.\text{unrooted} \leftarrow \text{true}$ 
   else
20:     for all  $u : uv \in E_W \wedge uv.\text{growth} = 1$  do
       if  $u.\text{CID} = \text{reset}$  then
22:         if not  $v.\text{unrooted}$  then
            $\triangleright \text{Start unrooting } v.$   $\triangleleft$ 
            $v.\text{busy} \leftarrow \text{true}$ 
            $v.\text{CID} \leftarrow \text{reset}$ 
            $v.\text{pointer} \leftarrow C$ 
           break
28:         else if  $u.\text{CID} < v.\text{CID}$  then
            $v.\text{busy} \leftarrow \text{true}$ 
            $v.\text{pointer} \leftarrow \text{toward } u$ 
            $v.\text{CID} \leftarrow u.\text{CID}$ 

```

In syncing, all defects are pushed along pointers toward roots, one edge per timestep (Lines 8 to 10). Eventually, each root will know using Lemma 1 whether its cluster is active (Line 4). At the same time, this activity knowledge propagates in the opposite direction from root to the rest of the cluster

(Line 7). After this process, a node is in an active cluster iff it is active.

Note that swapping the order of the two subroutines in MERGING would speed up the stage, as pointers would be updated *before* being used to push defects and backpropagate activity. However, the practicality of this depends on the hardware so in this paper we assume the worse case and perform SYNCING using pointers from the *previous* timestep.

B.2.2 Unrooting

Algorithms 3 and 4 also incorporate unrooting, a process unique to Snowflake. This is needed when a downward pointer is dropped to the bottom sheet of W (can happen while a cluster falls out of view). This breaks the pointer tree structure established in the previous decoding cycle, as \exists nonempty $S \subset V_W$ from which following the pointers will lead past the bottom of W . To fix it, each node in S resets its CID and pointer so that the structure can be rebuilt from scratch, via further merging timesteps. Figure 8 shows an example.

The breaking point is found before merging (Algorithm 3 Line 17) whence the signal to unroot, $\text{CID} = \text{reset}$, propagates during merging as a flood through the cluster; each node unroots itself as soon as it receives this signal (Algorithm 4 Lines 20 to 27). It takes 2 timesteps for a node to unroot, after which it cannot unroot again in the same decoding cycle (Algorithm 4 Line 22). This ensures the flood does not backpropagate. The memory of whether a node has unrooted resets after each merging stage (Algorithm 3 Line 2).

The higher up a node is in W , the lower its ID; this is for two reasons. First, it makes unrooting less likely as pointer paths tend to lead upward rather than downward. Second, it ensures defects in active clusters are pushed to a highest point so they can

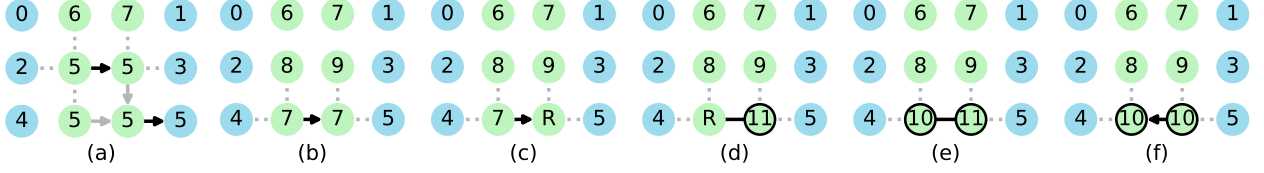


Figure 8: A decoding cycle which demonstrates unrooting. Relative variables are shown as in [Fig. 7](#). CID value reset is labelled 'R'. Nodes with unrooted as true are outlined in black. (a) There is a 5-node cluster. (b) During drop, a downward pointer is dropped to the bottom east detector. (c) Thus during grow, this detector starts unrooting. (d) merging starts. The bottom west detector sees this signal to unroot so starts unrooting. The bottom east detector finishes unrooting. (e) The bottom west detector finishes unrooting. (f) merging completes.

annihilate with defects in newer, smaller clusters as early as possible.